Somatic Gene Mutations Expose Cytoplasmic DNA to Co-Opt the cGAS-STING-NLRP3 Axis in Myelodysplastic Syndromes

Amy F. McLemore[1], Hsin-An Hou[2], Benjamin S. Meyer[1], Nghi B. Lam[1], Grace A. Ward[1,3], Amy L. Aldrich[1], Matthew A. Rodrigues[4], Alexis Vedder[1], Ling Zhang[5], Eric Padron[1], Nicole D. Vincelette[1], David A. Sallman[1], Omar Abdel-Wahab[6], Alan F. List[1,7] and Kathy McGraw[1,8]

1. Department of Malignant Hematology, Moffitt Cancer Center & Research institute, Tampa, FL
2. Department of Internal Medicine, National Taiwan University Hospital (NTUH), Taipei, Taiwan
3. Cancer Biology Ph.D. Department, University of South Florida, Tampa, FL
4. Luminex Corporation, Seattle, WA
5. Department of Hematopathology, Moffitt Cancer Center & Research institute, Tampa FL
6. Human Oncology and Pathogenesis Program and Leukemia Service, Memorial Sloan Kettering Cancer Center, New York, NY
7. Precision Biosciences, Durham, NC 27701
8. Laboratory of Receptor Biology and Gene Expression, National Cancer Institute, National Institutes of Health, Bethesda, Maryland 20892

Corresponding Author:

Kathy L. McGraw, Ph.D.
41 Medlars Drive
Bldg 41, B622
Bethesda, MD 20892
Email: Kathy.mcgraw@nih.gov
Phone: 240-760-7134

Abstract Word Count: 174

Text Word Count: 6948

Number of Figures: 7

Number of References: 47

Conflict of Interest

OA-W has served as a consultant for H3B Biomedicine, Foundation Medicine Inc, Merck, Prelude, and Janssen, and is on the Scientific Advisory Board of Envisagenics Inc and AIChemy and has received prior research funding from H3B Biomedicine unrelated to the current manuscript. AFL has provided consulting services to CTI Biopharma, Halia Therapeutics, Rigel Pharmaceuticals and Prelude Therapeutics and serves on the Scientific advisory board of Aileron. DS serves on the advisory board for Aprea, Bluebird Bio, BMS, Intellia, Kite, Novartis, Shattuck Labs, Servier, Syndax, is a consultant for AbbVie, Magenta, and Takeda, on the Speaker's Bureau for BMS, Incyte, and Servier, and receives research funding from Aprea and Jazz. DS, AFL also have potential royalty income from IP they developed related to cancer treatment. EP has research funding from BMS, Kura, Inctyte and honorarium from Novartis. MR is employed by Luminex Corporation, the maker of the Amnis ImageStream® used in this work.

Abstract

NLRP3 inflammasome and interferon stimulated gene (ISG) induction are key biological drivers of ineffective hematopoiesis and inflammation in Myelodysplastic Syndromes (MDS). Gene mutations involving messenger RNA splicing and epigenetic regulatory pathways induce inflammasome activation and myeloid lineage skewing in MDS through yet undefined mechanisms. Using immortalized murine hematopoietic stem and progenitor cells harboring these somatic gene mutations and primary MDS bone marrow specimens, we show accumulation of unresolved R-loops and micronuclei with concurrent activation of the cytosolic sensor, cGAS. cGAS-STING signaling caused interferon stimulated gene (ISG) induction, NLRP3 inflammasome activation, and maturation of the effector protease, caspase-1. Deregulation of RNA polymerase III drives cytosolic R-loop generation, which upon inhibition, extinguishes ISG and inflammasome response. Mechanistically, caspase-1 degrades the master erythroid transcription factor, GATA1, provoking anemia and myeloid lineage bias that is reversed by cGAS inhibition in vitro and in *Tet2*$^{-/-}$ hematopoietic stem and progenitor cell transplanted mice. Together, these data identity a novel mechanism by which functionally distinct mutations converge upon the cGAS-STING-NLRP3 axis in MDS directing ISG induction, pyroptosis and myeloid lineage skewing.

Introduction

Myelodysplastic syndromes (MDS) are genetically diverse hematopoietic stem cell malignancies characterized by ineffective and dysplastic hematopoiesis. Recent investigations provide convincing evidence that innate immune activation is a key driver of MDS pathogenesis. Hematopoietic stem and progenitor cells (HSPCs) overexpress Toll-like receptors (TLR) and generate inflammatory cytokines driving medullary expansion of hematopoietic-inhibitory, myeloid-derived suppressor cells (MDSCs).(1, 2) Innate immune signaling complexes known as supramolecular organizing centers (SMOCs) are constitutively active in MDS, including the TLR-MyDDosome and Nod-Like Receptor Protein 3 (NLRP3)-inflammasome complexes. These signaling modules induce transcription-dependent and -independent, inflammatory and lytic cell death responses. NLRP3 inflammasome activation drives both clonal expansion and pyroptotic cell death in MDS that manifests clinically as cytopenias.(3) Both cell-extrinsic and cell-intrinsic circuits appear to induce inflammasome assembly in MDS HSPCs. The myeloid-related S100A9 protein and other danger-associated molecular patterns (DAMPs) released upon cytolysis induce canonical inflammasome activation through TLRs in a feed-forward, receptor-driven fashion. Notably, somatic gene mutations involved in mRNA splicing and epigenetic regulation, the most commonly mutated gene classes in MDS, also evoke NLRP3 inflammasome activation in human and murine models.(3) These findings suggest that somatic mutations affecting functionally diverse gene classes may converge upon a common pathway for cell-intrinsic inflammasome activation in MDS.

One possible mechanism by which somatic gene mutations lead to inflammasome activation is through augmented genome instability.(4, 5) Somatic mutations evoke replication stress resulting in transcriptional pauses exposing genomic DNA to cytosolic sensors through accumulation of unresolved R-loops or formation of fragile micronuclei.(6, 7) Importantly, HSPC gene expression profiling has shown Type I interferons and interferon-stimulated genes (ISGs) are the most highly

expressed genes in MDS(8), consistent with datasets from mutant-*U2AF1* [GSE66793] and *Tet2*$^{-/-}$ mouse RNAseq studies [GSE27816]. Sustained Type I interferon signaling in murine models results in excess interleukin (IL)-1β elaboration, ineffective hematopoiesis, and bone marrow failure.(9) With the exception of TLR4, all other intracellular pattern recognition receptors that induce type I interferons are nucleic acid sensors activating the interferon regulatory factor (IRF)-3 or IRF7 transcription factors. Although multiple cytosolic DNA sensors can potentially trigger a type I interferon response, including the Absent in Melanoma 2 (AIM2)-like receptors (ALR) and its family member IFI16, CRISPR-editing and murine models show ALRs are dispensable for intracellular DNA interferon response, whereas cyclic GMP-AMP Synthase (cGAS) is indispensable.(10, 11) cGAS and the Stimulator of Interferon Genes (cGAS-STING) form a cell-intrinsic DNA surveillance pathway that recognizes cytosolic DNA leading to ISG transcription and NLRP3 inflammasome activation.(12, 13) Further, recent data demonstrates that cGAS induced ISG expression is responsible for defective hematopoiesis in in vivo models.(14) cGAS dimerizes upon dsDNA engagement catalyzing generation of 2',3'-cyclic-GMP-AMP (cGAMP) that binds to and activates STING.(12) STING is essential for inflammasome activation in response to cytosolic DNA exposure promoting activation in two ways. First, STING binds NLRP3 in the endoplasmic reticulum where it anchors the nod-like receptor for speck assembly and caspase-1 cleavage.(15) Secondly, STING represses polyubiquitination of NLRP3 which is necessary for inflammasome activation.(16)

Here, we investigated sources of cytoplasmic DNA exposure to nucleic acid sensors in primary MDS BM specimens and functionally distinct murine gene mutation models as possible common cell-intrinsic platforms licensing the NLRP3 inflammasome. We report that both RNA splicing and epigenetic modifying gene mutations expose redundant sources of cytoplasmic DNA to cytosolic cGAS-STING that drives Type I interferon response, NLRP3 inflammasome activation, pyroptotic cell death and caspase-1 directed myeloid lineage skewing, which is rescued by cGAS genetic

and pharmacologic inhibition. These findings suggest that inhibition of the cGAS-STING-NLRP3 signaling axis may represent a novel therapeutic strategy for investigation in MDS.

Results

Somatic gene mutations provoke cytosolic DNA exposure

To investigate the mechanisms by which SGM evoke inflammasome activation, we first generated renewable cell sources carrying specific mutations common to MDS by immortalizing BM-HSPC from *Tet2*$^{-/-}$ and *Srsf2*^{P95H} mutant and respective wild type (WT) control mice. These common MDS mutations have been demonstrated to induce innate immune activation leading to pro-inflammatory cytokine elaboration in MDS. The immortalized cell lines maintain progenitor phenotypes suitable for investigation and were validated prior to experimentation (**Supplemental Figure S1**).(3, 17, 18) To confirm that these models phenocopy human MDS, we first evaluated inflammasome activity that we previously demonstrated is a key driver of MDS pathogenesis.(3) Both mutant models displayed increased caspase-1 cleavage assessed by the Caspase-Glo® 1 assay compared to wild type (WT) controls, indicative of NLRP3 inflammasome assembly and caspase-1 activation ($P < 0.0001$ for both mutations) (**Figure 1A**). We next sought to determine whether these mutations caused accumulation of genotoxic stress markers. Micronuclei can be found under conditions of nuclear stress and are formed from lagging mitotic chromosomal DNA and chromatin bridges. We found that both mutant HSPC models displayed a significantly higher mean percentage of micronuclei compared to WT cells (*Tet2,* $P = 0.0090$; *Srsf2,* $P = 0.0001$;) (**Figure 1B**). To determine if these findings were consistent with human MDS, we compared primary BM specimens from MDS patients (n=8) and healthy donors (n=6). Primary MDS specimens displayed a significantly higher fraction of cells containing micronuclei compared to age-matched controls, indicating that the murine mutation variants faithfully recapitulate the findings in human MDS ($P = 0.0068$) (**Figure 1C**). Impaired micronuclei membrane integrity often leads to membrane collapse and leakage of DNA into the cytosol, therefore, we assessed Lamin

B1 staining which demonstrated micronuclear envelopes were noticeably thinner compared to nuclear membranes potentially indicative of membrane collapse and DNA compartmentalization compromise (**Figure 1D**). Additional sources of genomic DNA resolved by replicative stress and transcriptional pauses arising from SGMs can also augment accumulation of DNA:RNA hybrids, or R-loops.(6) Using the S9.6 antibody that recognizes RNA:DNA hybrids(19), flow cytometry demonstrated a significant increase in cellular R-loops in both of the SGM models studied (*Tet2,* $P = 0.0011$; *Srsf2,* $P < 0.0030$) (**Figure 1E**). These findings were confirmed by immunofluorescence in MDS BM-MNC ($n = 6$) compared with healthy donors ($n = 3$) ($P = 0.0264$) (**Figure 1F, G**). Of particular interest, although R-loops were visualized in the nuclei, R-loop immunostaining was largely cytoplasmic. Thus, cytosolic DNA sensors may access genomic DNA in MDS progenitors through two sources, unresolved R-loops and structurally unstable micronuclei that are induced by both mRNA splicing and epigenetic regulatory gene mutations.

cGAS is activated by cytoplasmic DNA in MDS

Type I interferons block maturation of HSPCs, a process that is attenuated by inhibition of the cytosolic DNA sensor, cGAS.(14) Given the increased prevalence of micronuclei that may expose genomic DNA through porous nuclear membranes, and accumulation of cytosolic R-loops in our murine models and primary specimens, we next examined whether cGAS engages these sources of cytoplasmic DNA. We first used immunofluorescence staining to demonstrate cGAS co-localization with both micronuclei (**Figure 2A**) and cytoplasmic R-loops (**Figure 2B**) and indeed found that cGAS interacted with both in MDS BM-MNCs as well as the murine mutation variants. Upon engagement with DNA, cGAS dimerizes to catalyze synthesis of the second messenger 2'-3' cGAMP that binds to and activates STING. cGAS engagement of DNA results in the formation of punctate catalytic foci that coalesce into larger spherical droplets by liquid phase transition.(20) Accordingly, cGAS foci were observed in murine SGM cells and MDS primary specimens while limited or absent from wildtype or normal controls, confirming cGAS dimerization and activation

upon DNA engagement (**Figure 2C, D**). Upon cGAMP activation, STING translocates from the endoplasmic reticulum to the perinuclear trans-Golgi network permitting its tetramerization and recruitment of Tank-Binding Kinase 1 (TBK1). TBK1 oligomerizes and autophosphorylates which enables recruitment and phosphorylation of the transcription factor IRF3, and together with the IKKε kinase, NF-kB. Phospho-IRF3 dimerizes and translocates to the nucleus to direct transcription of interferon-β and ISGs.(21) Flow cytometry showed that phosphorylation of IRF3 was significantly increased in both murine SGM variants compared to wildtype controls (*Tet2,* P = 0.0002; *Srsf2,* P = 0.0058) (**Figure 2E**). Accordingly, gene expression of the ISGs, *Ccl5* and *Cxcl10*, was elevated in the mutant variants compared to wild type controls (**Figure 2F**), consistent with findings in the MDS primary specimens (*CXCL10*, P = 0.013; *ISG15*, P < 0.0001; *SAMD9L*, P = 0.0007; *IFI27L2*, P < 0.0001; *IFNB1*, P < 0.0001) (**Figure 2G**). To confirm that the cGAS-STING pathway is responsible for this ISG induction, we treated cells with the cGAS inhibitor, RU.521, which selectively suppresses cGAS catalytic activity without affecting retinoic acid-inducible gene (RIG)-1, TLR-2, -3, -4, or Janus Kinase (JAK)/Signal Transducer and Activator of Transcription (STAT) signaling.(22) Indeed, pharmacologic inhibition of cGAS significantly reduced *Ccl5* expression in SGM models to levels comparable of that found in wildtype controls (*Tet2*, P = 0.0004; *Srsf2*, P = 0.0480) (**Figure 3A**). These studies were validated in primary MDS specimens where RU.521 treatment significantly reduced IRF3 phosphorylation (**Figure 3B**), with corresponding suppression of *IFNB1, CXCL10 and SAMD9L* gene messages in primary MDS specimens (*IFNB1,* P = 0.0651; *CXCL10,* P = 0.0367; *SAMD9L,* P = 0.0073) (**Figure 3C**). Collectively these data indicate that cytoplasmic DNA exposed by SGMs engages and activates a cGAS-STING-Type I interferon response in MDS.

cGAS-STING signaling induces NLRP3 inflammasome activation

Gaidt *et al.* and others demonstrated that the cGAS-STING pathway is essential for NLRP3 inflammasome activation in response to cytosolic DNA exposure in myeloid cells.(13, 23) From

the trans-Golgi network, STING transitions to the lysosome where it permeabilizes the lysosomal membrane triggering cathepsin B and Ca^{2+} ion release with the consequent activation of the calcium/calmodulin-dependent protein kinase type II (CaMKII)-TAK1-JNK pathway that activates the NLRP3 inflammasome.(23) To determine if cGAS-STING functions as the principal cell-autonomous pathway provoking inflammasome activation by SGMs, we treated the murine SGM HSPC variants with the cGAS inhibitor, RU.521. Incubation of SGM models with RU.521 reduced caspase-1 cleavage in a concentration dependent manner (**Figure 3D**), demonstrating cGAS-STING regulates NLRP3 inflammasome activation by SGMs. Moreover, total levels of pro-caspase-1 were concordantly reduced, consistent with the known transcriptional priming of NLRP3 inflammasome components by Type I interferons.(13) To confirm that these findings were not due to nonspecific effects of pharmacologic perturbation, we used CRISPR gene editing to knockout *cGAS* expression in the immortalized *Tet2*$^{-/-}$ HSPC cells. We used two unique cGAS gRNAs (sg_3 and sg_4) in the *Tet2*$^{-/-}$ cells and compared this to transduction of a scrambled gRNA in WT and *Tet2*$^{-/-}$ cells. Cells were transduced with guide containing lentivirus and expanded after GFP sorting. Indeed, protein expression of cGAS was nearly completely abolished using both sg_3 and sg_4 (**Figure 3E**). Similar to pharmacologic inhibition, cGAS knockdown by gene editing resulted in a decrease in ISG expression, returning *Ccl5* mRNA expression in *Tet2*$^{-/-}$ cells to levels commensurate with wild type (**Figure 3F**). Decreased ISG expression was accompanied by a corresponding reduction in IRF3 activity demonstrated by decreased nuclear localization of the transcription factor (**Figure 3G**). Importantly, CRISPR knockdown of *cGAS* also suppressed capase-1 activity, further indicating that cGAS-STING directs inflammasome activation in response to cytoplasmic DNA sources exposed by SGMs (**Figure 3H**). These findings were then validated by treatment of primary MDS BM-MNC with RU.521, which suppressed inflammasome activity as evidenced by a reduction in caspase-1 cleavage, IL-1β maturation and generation of ASC specks, a reliable surrogate for inflammasome activity (24) (**Figure 4A, B**). Lastly, knockdown of *cGAS* with shRNA in 3 primary MDS specimens consistently

showed a marked reduction in caspase-1 cleavage (**Figure 4C-E**), confirming that cGAS engagement of DNA licenses NLRP3 inflammasome activation in MDS.

Cytosolic R-loops are evoked by RNA polymerase 3

Nuclear RNA:DNA hybrids are transcribed largely by RNA polymerase (RNAP) II,(25) however, recent investigations have shown that RNA:DNA hybrids are also demonstrable in the cytosol of human tumor cells of varied histogenic origin. These cytosolic R-loops are generated by RNA polymerase III (RNAP3) and exported to the cytosol by the nuclear pore transport protein, exportin-1.(26) RNAP3 transcribes 5S rRNA, tRNA, certain retroelements and noncoding RNAs, and is regulated by oncogenes and tumor suppressor genes. In one study, inhibition of RNAP3 and not DNA polymerases, was sufficient to abolish cytosolic RNA:DNA hybrid generation, indicating that RNAP3 transcripts may be the source of cytosolic RNA:DNA hybrids recognized by cGAS.(26) To determine if the excess accumulation of cytosolic R-loops induced by SGMs is transcribed by RNAP3; and whether they are sufficient to license cGAS induced inflammasome oligomerization, we first investigated RNAP3 gene expression. Microarray expression of each RNAP3 subunit was found to be significantly elevated in MDS specimens compared to controls (**Supplemental Table S1**). To determine whether RNAP3 is responsible for the accumulation of R-loops in SGM variants and MDS cases, we incubated cells with the highly specific RNAP3 inhibitor, ML-60218, and assessed changes in R-loop accumulation and inflammasome activity. ML-60218 treatment of the immortalized SGM HSPCs markedly suppressed cellular R-loops assessed by flow cytometry (**Figure 5A**) and immunofluorescence (**Figure 5B, C**). Accordingly, we found that R-loop suppression by ML-60218 abolished caspase-1 cleavage, indicating that DNA:RNA hybrids generated by RNAP3 may be the predominant source of cytosolic DNA inducing DNA-directed, inflammasome activation by SGMs (**Figure 5D**). We next treated primary MDS specimens (n=3) with ML-60218, which significantly reduced R-loops (P = 0.0381) (**Figure 5E**) in addition to *IFNB1* and *SAMD9L*, but not *CXCL10* expression (*IFNB1,* P = 0.0050; *SAMD9L,*

P = 0.0150) (**Figure 5F**). Treatment also significantly reduced active caspase-1, IL-1β, and ASC specks (P = 0.0162, 0.0050, 0.0016, respectively) (**Figure 5G**), indicating that RNAP3 inhibition attenuates inflammasome activity in primary MDS specimens. Overall, these data indicate that SGM deregulate RNAP3 in MDS, resulting in excess cytoplasmic R-loop generation that is engaged by cGAS-STING.

cGAS-STING-NLRP3 signaling directs myeloid lineage bias by SGMs

The mRNA splicing and epigenetic modifying gene mutations common to MDS promote granulo-monocytic skewing at the expense of erythroid differentiation.(27-30) Erythroid versus myeloid lineage fate is governed by the balance of the GATA binding protein 1 (GATA1) and the *Spi1*-encoded PU.1 transcription factors, respectively, that physically interact and mutually repress respective target genes.(31) Caspase-1 regulates erythroid:myeloid lineage bias through degradation of the master erythroid transcription factor, GATA1, thereby raising the PU.1/GATA1 ratio to favor myeloid commitment.(32) To determine if inflammasome activation by cGAS drives myeloid lineage skewing, we treated HSPC with the cGAS inhibitor, RU.521. Treatment of primary MDS specimens resulted in marked upregulation of *GATA1* (P = 0.0159) (**Figure 6A**) accompanied by expansion of erythroid precursors (**Figure 6B**) and increased expression of the CD71 transferrin receptor (P = 0.0338) (**Figure 6C**), indicating reversal of myeloid lineage skewing. To confirm the functional role of the cGAS-STING-NLRP3 axis in vivo, we transplanted *Tet2*$^{fl/fl}$ CD45.2 donor BM-MNC into CD45.1 recipient mice and began daily treatment with RU.521 (10mg/kg by intraperitoneal injection) at 14 weeks. After 6 weeks of treatment with the cGAS inhibitor, ASC speck percentage of CD45.2 cells was significantly reduced with a corresponding increase in the erythroid compartment demonstrated by hematoxylin and eosin staining of murine femurs (**Figure 6D, E**). Further, cGAS inhibition caused statistically significant increases in hemoglobin (P = 0.0323) and hematocrit (P = 0.0453) accompanied by a reduction in monocytes (P = 0.0626) and rise in lymphocytes (P = 0.0319) (**Figure 6F**). These data indicate that myeloid

lineage skewing by SGMs arises from activation of the cGAS-STING-NLRP3 axis that directs caspase-1 mediated degradation of GATA1.

Discussion

Somatic mutations involving mRNA splicing or epigenetic regulatory genes are the most common genetic abnormalities in MDS. Although frequently co-occurring, individual gene mutations from either of these functionally distinct classes are singularly sufficient to induce NLRP3 inflammasome activation, which drives ineffective hematopoiesis through pyroptotic cell death.(3) To our knowledge, our investigations demonstrate for the first time that these mutations converge upon the cGAS-STING-NLRP3 signaling axis as a common pathway directing inflammasome activation in MDS (**Figure 7**). We show the cytosolic DNA sensor, cGAS, engages unresolved R-loops and structurally unstable micronuclei in murine mutation models and MDS HSPC. cGAS-STING activation leads to transcription factor, IRF3, activation directing Type I interferon response and ISGs transcription. cGAS genetic or pharmacologic inactivation extinguished ISG expression and caspase-1 cleavage indicating that this signaling axis is singularly responsible for interferon and inflammasome induction. Particularly important, licensing of cGAS-STING-NLRP3 by exposed cytoplasmic DNA provides a mechanistic rationale for inflammasome induction in age-related clonal hematopoiesis, which accelerates atherosclerotic plaque formation and cardiovascular risk.(33, 34) Although other nucleic acid sensors recognizing dsRNA might also detect R-loops, these receptors exhibit a preference for non-self RNA or are localized in endolysosomal compartments where they are shielded from endogenous RNA. These findings also provide a mechanistic rationale for findings by Zhou *et al*. that accumulation of cytosolic dsDNA in senescent cells triggers the induction of pyroptosis.(35) Although we found that cGAS engages both micronuclei and R-loops, the latter appear to be the principal source of DNA driving cGAS-STING-NLRP3 signaling. While R-loops were demonstrable in the nuclei of mutant and MDS HSPC, they were abundantly cytosolic permitting cGAS engagement. Surprisingly, cytosolic

R-loops were largely generated by RNAP3, evidenced by R-loop depletion, and extinction of ISG and inflammasome response upon RNAP3 inhibition.

Murine models have shown that mRNA splicing and epigenetic modifying gene mutations promote myeloid lineage skewing at the expense of erythroid differentiation.(27-30) Here, we report myeloid lineage skewing induced by somatic gene mutations arises from caspase-1 mediated degradation of GATA1. The balance between GATA1 and the myeloid transcription factor PU.1 governs lineage commitment; therefore, degradation of GATA1 favors myeloid skewing.(32, 36) Indeed, MDS HSPC incubation with a potent cGAS inhibitor stabilized GATA1 and induced erythroid expansion. In a *Tet2*-deficient mouse HSPC transplant model, we found cGAS inhibition restored hemoglobin production, resolved anemia, and suppressed monocyte production. Our findings that myeloid lineage skewing by somatic mutations arises from caspase-1 degradation of GATA1 enabled by the cGAS-STING-NLRP3 axis provides mechanistic rationale for the recent report that oncogenic *Kras*^{G12D} induces myeloproliferation as a result of NLRP3 inflammasome activation.(37)

Recent reports have shown that MDS HPSCs harboring somatic gene mutations activate non-canonical NF-kB signaling to confer a competitive advantage in the inflammatory MDS microenvironment.(38) This inflammation-directed activation of alternative NF-κB signaling was dependent upon upregulation of the ubiquitin-modifying enzyme A20 encoded by the ISG, *TNFAIP3*. Through its binding to and dissociation of the NF-κB-inducing kinase (NIK)-polyubiquitination complex, A20 provokes degradation of tumor necrosis factor (TNF) receptor-associated factor 2 (TRAF2) and TRAF3 to stabilize NIK.(39) Activation of the cGAS-STING-IRF3 axis triggers degradation of TRAF3, thereby stabilizing NIK and activating the non-canonical NF-kB signaling pathway.(40) Upon autophosphorylation, NIK oligomerizes and associates with the STING-TBK1-IRF3 complex. NIK binding suppresses decoration of STING with K48-linked

ubiquitin chains enhancing stability and strengthening Type I interferon response. Weinreb *et a*l recently reported that excess R-loops engage cGAS-STING to trigger an inflammatory cascade that directs an increase in HSPC production, thereby endowing a self-renewal benefit to mutant HSPC.(41) Importantly, the data here provide a mechanistic rationale for the concurrent induction of NLRP3 inflammasome-enabled caspase-1 activation, myeloid skewing and the competitive renewal advantage of clonal HSPCs in the inflammatory MDS microenvironment. Together, these investigations suggest that inhibition of the cGAS-STING-NLRP3 signaling axis may represent a promising therapeutic strategy for investigation in MDS.

Material and Methods

Cells

Bone marrow mononuclear cells (BM-MNC) cells harvested from *Tet2*$^{-/-}$ and *Srsf2*^{P95H} mutant mice and their respective wildtype (WT) controls were immortalized for use as MDS somatic gene mutation (SGM) cell line models.(42, 43) Murine cells were immortalized using a conditional *Hoxb8* transgene as previously described.(44) Briefly, BM-MNC were harvested from mice and transduced with an estrogen regulated (ER)-HoxB8 containing retrovirus and cultured in RPMI supplemented with 10% FBS, 1% pen/strep, 50 ng/mL recombinant murine stem cell factor, and 0.5 µM beta-estradiol. Primary BM-MNC were isolated using Ficoll®-Paque (GE Healthcare, Chicago, IL) from MDS patients and healthy donors who provided informed consent at the Moffitt Cancer Center or the National Taiwan University Hospital or purchased from Allcells (Alameda, CA). Primary BM-MNCs were cultured in RPMI supplemented with 10% autologous plasma. Cells were treated with the cGAS inhibitor RU.521 (Aobious, Gloucester, MA) or RNA Polymerase III inhibitor (RNAP3i) ML-60218 (EMD Millipore, Burlington, MA) at 1 µM or 10 µM, respectively, for 24 - 72 hr.

Dot blotting

DNA was extracted using QIAamp DNA Mini Kit (Qiagen) following manufacturer's protocol and denatured for 5 min at 99°C then placed on ice for 10 min. DNA was neutralized by adding one volume of 2M ammonium sulfate pH 7.0 and incubating on ice for 5 min. Samples were then sonicated for 30 sec, quantitated, and diluted to equal concentrations. Two µg of DNA was dotted on the membrane and allowed to fully dry. Membranes were then crosslinked with UV and blocked in 10% non-fat dry milk for 15-20 min then incubated in 5-hmC primary antibody (Active Motif, 1:1000) for 15 min. The membrane was then washed 3x times at RT with PBST and incubated in 1:5000 secondary antibody for 15 min at RT. The membrane was then washed and developed using chemiluminescence. The membrane was then washed in 0.4 µg/mL of propidium iodide, washed with PBS, and imaged.

PCR sequencing for cell line validation

SRSF2^{P95H} mutation was confirmed by PCR amplification of cDNA using forward primer 5' ACGTGTACATTCCGCGGGAC 3' and reverse primer 5' ATCTGGAGACGGAGGAGGAC 3' with the following amplification, 94°C for 2 min then 35 cycles of 94°C for 30 sec, 55°C for 30 sec, 72°C or 30 sec and a final extension at 72°C for 5 min.

Oligonucleotides and Antibodies

All qPCR primers and sgRNAs are listed in **Supplemental Table S2**, and all antibodies are listed in **Supplemental Table S3**.

Western Blotting

Cells were harvested and washed 3 times in PBS then lysed using 1× RIPA buffer containing 250 µM NaVO4, 2 µg/ml aprotinin, 2 µg/ml leupeptin, 0.2 µg/ml pepstatin A, and 500 µM PMSF. Proteins were separated by SDS-PAGE and transferred onto PVDF membranes. Membranes

were blocked with 5% non-fat dry milk in PBST, then incubated with indicated antibodies. Membranes were developed using ECL or ECL+ per manufacturer's protocol.

Active Caspase-Glo® 1 Assay

Cell culture supernatants were used to measure active caspase-1 using the *Caspase-Glo® 1* (Promega, Madison, WI) per manufacturer protocol.

CRISPR-Cas9 gene editing

cGAS genes were deleted by CRIPSR-Cas9 gene editing by inserting one of two different *cGAS*, or 1 scrambled guide RNA into a green fluorescent protein (GFP)-expressing pL-CRISPR.SFFV.GFP plasmid (pL-CRISPR.SFFV.GFP that was a gift from Benjamin Ebert (Addgene plasmid # 57827 ; http://n2t.net/addgene:57827 ; RRID:Addgene_57827).(45) The plasmid was digested using BsmBI and gel purified. Forward and reverse guide oligonucleotides were purchased from Integrated DNA Technologies (Coralville, IA). CACC on forward and AAAC on reverse oligonucleotides were added 5' for plasmid ligation. Guide containing plasmids were transformed into Stbl3 competent cells. CRISPR plasmids were packaged into lentivirus using HEK293T cells transfected by incubating 2600 ng of shRNA plasmid, 30 µL Lipofectamine® 2000 (Invitrogen), 26 µL MISSION™ Lentiviral Packaging Mix (Sigma) in 500 µL of Opti-MEM®I (Life Technologies) for 15 min at room temperature. This mixture was then added to 70% confluent HEK293T cells with 4 mL serum-free Opti-MEM® medium in a 100 mm dish. Viral containing supernatants were collected 48hr and 72hr post transfection. Lentiviral transduction of immortalized murine cells was performed by spinfection (3000 rpm for 2 hr) method (1 mL virus with titer of at least 10^5 IFU/mL added to 500 µL containing 250,000 cells per well in a 24 well plate) with 8 µg/mL polybrene. After spinfection, cells were incubated at 37 °C in a humidified incubator (5% CO_2) for 1 hr, then 3 mL of complete media (RPMI with 10% FBS, 1% pen/strep, 50 ng/mL recombinant murine stem cell factor, and 0.5 µM beta-estradiol) was added. After 3

days, GFP+ cells were sorted and expanded. Cells were cultured in complete media and harvested for downstream assays.

Immunofluorescence Microscopy

Cytospins were fixed with Cytofix (BD, Franklin Lakes, New Jersey), 10 minutes, 37°C, washed with 0.1 M Glycine (Fisher Scientific, Hampton, NH) and PBS, permeabilized/blocked with 0.2% Triton-X100/2% BSA, 30 min at RT. Primary antibody staining, 1 hr at RT, 3x wash, secondary antibodies, 1 hr at RT. Cells were mounted with ProLong Gold Antifade Mountant with DAPI (Invitrogen, Carlsbad, CA) and imaged using a Leica SP8 confocal microscope (Wetzlar, Germany). At least 100 cells were assessed for each replicate.

Quantitation of ASC Specks

Primary BM-MNCs were fixed with BD Cytofix for 10 min, washed with 0.1M Glycine, permeabilized/ blocked with 0.2% Triton-X100/2% normal mouse serum (Abcam, Cambridge, MA) 1 hr, stained with mAB ASC conjugated to AF647 (Santa Cruz Biotechnology, Dallas, TX) 1 hr, and resuspended in 1 µg/mL DAPI (Sigma-Aldrich). Data were acquired with Amnis ImageStream$^{X®}$ Mark II imaging flow cytometer and analyzed using IDEAS® (Luminex, Austin, TX). Data were analyzed as previously described(46) with modifications. Samples were run on the lowest speed and at least 3000 images were collected with 60x objective. A masking strategy was applied to remove doublets, identify ASC speck containing cells, and differentiate specks from diffuse staining.

Murine studies

BM-MNC were harvested from 3-5 week old *Tet2*$^{fl/fl}$ donor mice (The Jackson Laboratories, Bar Harbor, ME, Stock No:017573). CD45.1 recipient mice (Stock No:002014) were sub-lethally irradiated with 6 Gy for 24 hours prior to transplant. At transplant, donor cells were thawed and

washed with 10 mL IMDM. Cells were then treated with 0.1 mg/mL DNAse, 15 min, at RT. One million cells in 100 µL saline were tail vein injected per mouse. Mice were induced with 250 µg pI:pC twice every other day 7 days post injection. Mice with at least 70% CD45.2 repopulation were used. Mice were treated with vehicle (5% NMP, 5% Solutol, 90% Saline) or 10 mg/kg RU.521 by intraperitoneal injection 1x/day, 7day/week for 6 weeks at 14 weeks post-induction. Tissues were fixed in formalin for 48 hr then preserved in 70% ethanol until analysis.

Gene expression analysis

RNA was extracted by Qiagen RNeasy Mini Kit (Hilden, Germany) and reverse transcribed using qScript XLT cDNA Supermix (QuantaBio, Beverly, MA). *INFB1/Infb1 and GATA1* was quantified using TaqMan Advanced Gene Expression Assays, TaqMan Fast Advanced Master Mix, and 7900HT Fast Real-Time PCR System (Life Technologies, Foster City, CA). *ISG15/Isg15, CXCL10/Cxcl10, SAMD9L, and Ccl5* expression were quantified with primers listed in **Supplemental Table S2** and SYBR Green PCR Master Mix (Life Technologies). Ct values were normalized to *ACTB*/*Actb* for TaqMan and *GAPDH/Gapdh* for SYBR assays, delta-delta Ct method calculated fold-change. Gene expression profiling was also obtained from 213 MDS patients and 20 healthy donors from the NTUH using HumanHT-12 v4 Expression BeadChip (Illumina, San Diego, CA).(47)

shRNA

cGAS shRNA constructs were purchased from Origene (cat# TL305813, Rockville, MD) and packaged into as previously described.(3) shRNAs were used either as single shRNAs (shRNA A, B, C, or D) or pooled (equal concentrations of shRNA A-D) and conditions with the greatest reduction in expression of cGAS assessed by flow, which varied amongst cases, was used for analysis.

Flow Cytometry

For active caspase-1, -3/7 staining, cells were washed with PBS/2% FBS and incubated with either FAM-FLICA or FLICA 660 (ImmunoChemistry Technologies, Bloomington, MN) per manufacturer protocol. For fixable viability staining, cells were washed, stained with Zombie NIR, Violet, or Ultraviolet (BioLegend, San Diego, CA), 15 min, 1:1000 dilution, at RT then washed with PBS/2% FBS. For antibody staining, cells were incubated with human or mouse Fc block (Miltenyi, Bergisch Gladbach, Germany), stained 20 min at 4 °C. Data were acquired using a BD Symphony, Canto, or LSRII flow cytometer (BD, Franklin Lakes, New Jersey). FCS files were analyzed using FlowJo v10 software (Tree Star, Ashland, OR). Relative MFIs between replicates were compared as fold change differences rather than raw MFI values due to variation between flow cytometer machines.

Statistical Methods

Student t-test was used to compare means for in vitro and in vivo experiments. Statistical analyses were performed using Prism (GraphPad, San Diego, CA). Mann-Whitney U test was used to compare median expression of ISGs in MDS patient specimens compared to BM donors. Statistical analyses were performed by using SPSS 23 software (IBM Corporation, Armonk, NY). Unless otherwise indicated, data are presented as mean +/- standard deviation. P-values less than 0.05 were considered statistically significant.

Study Approval

Written informed consent was acquired for all patient samples and animal studies were performed according to IACUC approved protocols.

Author Contributions

AFM, AFL, KLM wrote the manuscript. AFM, HH, BSM, NL, GAW, ALA, AV, LZ, NDV, KLM performed experiments and analyzed data. MAR, EP, DS, OAW analyzed data.

Acknowledgements

This work has been supported in part by the Flow Cytometry, Analytic Microscopy, and Tissue Core Facilities at the Moffitt Cancer, an NCI designated Comprehensive Cancer Center (P30-CA076292). This work was also supported by funding provided by the Leukemia and Lymphoma Society (7018-19). The graphical abstract was created with BioRender.com.

References

1. Chen X, Eksioglu EA, Zhou J, Zhang L, Djeu J, Fortenbery N, et al. Induction of myelodysplasia by myeloid-derived suppressor cells. J Clin Invest. 2013;123(11):4595-611.

2. Maratheftis CI, Andreakos E, Moutsopoulos HM, Voulgarelis M. Toll-like receptor-4 is up-regulated in hematopoietic progenitor cells and contributes to increased apoptosis in myelodysplastic syndromes. Clin Cancer Res. 2007;13(4):1154-60.

3. Basiorka AA, McGraw KL, Eksioglu EA, Chen X, Johnson J, Zhang L, et al. The NLRP3 inflammasome functions as a driver of the myelodysplastic syndrome phenotype. Blood. 2016;128(25):2960-75.

4. Mahfoudhi E, Talhaoui I, Cabagnols X, Della Valle V, Secardin L, Rameau P, et al. TET2-mediated 5-hydroxymethylcytosine induces genetic instability and mutagenesis. DNA Repair (Amst). 2016;43:78-88.

5. Xiao R, Sun Y, Ding JH, Lin S, Rose DW, Rosenfeld MG, et al. Splicing regulator SC35 is essential for genomic stability and cell proliferation during mammalian organogenesis. Mol Cell Biol. 2007;27(15):5393-402.

6. Chen L, Chen JY, Huang YJ, Gu Y, Qiu J, Qian H, et al. The Augmented R-Loop Is a Unifying Mechanism for Myelodysplastic Syndromes Induced by High-Risk Splicing Factor Mutations. Mol Cell. 2018;69(3):412-25 e6.

7. Mackenzie KJ, Carroll P, Martin CA, Murina O, Fluteau A, Simpson DJ, et al. cGAS surveillance of micronuclei links genome instability to innate immunity. Nature. 2017;548(7668):461-5.

8. Pellagatti A, Cazzola M, Giagounidis AA, Malcovati L, Porta MG, Killick S, et al. Gene expression profiles of CD34+ cells in myelodysplastic syndromes: involvement of interferon-stimulated genes and correlation to FAB subtype and karyotype. Blood. 2006;108(1):337-45.

9. Dauphinee SM, Richer E, Eva MM, McIntosh F, Paquet M, Dangoor D, et al. Contribution of increased ISG15, ISGylation and deregulated type I IFN signaling in Usp18 mutant mice during the course of bacterial infections. Genes Immun. 2014;15(5):282-92.

10. Choubey D, Panchanathan R. IFI16, an amplifier of DNA-damage response: Role in cellular senescence and aging-associated inflammatory diseases. Ageing Res Rev. 2016;28:27-36.

11. Gray EE, Winship D, Snyder JM, Child SJ, Geballe AP, Stetson DB. The AIM2-like Receptors Are Dispensable for the Interferon Response to Intracellular DNA. Immunity. 2016;45(2):255-66.

12. Sun L, Wu J, Du F, Chen X, Chen ZJ. Cyclic GMP-AMP synthase is a cytosolic DNA sensor that activates the type I interferon pathway. Science (New York, NY). 2013;339(6121):786-91.

13. Swanson KV, Junkins RD, Kurkjian CJ, Holley-Guthrie E, Pendse AA, El Morabiti R, et al. A noncanonical function of cGAMP in inflammasome priming and activation. J Exp Med. 2017;214(12):3611-26.

14. Geng X, Zhang C, Li M, Wang J, Ji F, Feng H, et al. PICH Supports Embryonic Hematopoiesis by Suppressing a cGAS-STING-Mediated Interferon Response. Adv Sci (Weinh). 2022:e2103837.

15. Wang W, Hu D, Wu C, Feng Y, Li A, Liu W, et al. STING promotes NLRP3 localization in ER and facilitates NLRP3 deubiquitination to activate the inflammasome upon HSV-1 infection. PLoS Pathog. 2020;16(3):e1008335.

16. Humphries F, Bergin R, Jackson R, Delagic N, Wang B, Yang S, et al. The E3 ubiquitin ligase Pellino2 mediates priming of the NLRP3 inflammasome. Nat Commun. 2018;9(1):1560.

17. Pollyea DA, Harris C, Rabe JL, Hedin BR, De Arras L, Katz S, et al. Myelodysplastic syndrome-associated spliceosome gene mutations enhance innate immune signaling. Haematologica. 2019;104(9):e388-e92.

18. Jeong JJ, Gu X, Nie J, Sundaravel S, Liu H, Kuo W-L, et al. Cytokine-Regulated Phosphorylation and Activation of TET2 by JAK2 in Hematopoiesis. Cancer Discovery. 2019;9(6):778-95.

19. Sanz LA, Chedin F. High-resolution, strand-specific R-loop mapping via S9.6-based DNA-RNA immunoprecipitation and high-throughput sequencing. Nat Protoc. 2019;14(6):1734-55.

20. Du M, Chen ZJ. DNA-induced liquid phase condensation of cGAS activates innate immune signaling. Science (New York, NY). 2018;361(6403):704-9.

21. Mukai K, Konno H, Akiba T, Uemura T, Waguri S, Kobayashi T, et al. Activation of STING requires palmitoylation at the Golgi. Nat Commun. 2016;7:11932.

22. Vincent J, Adura C, Gao P, Luz A, Lama L, Asano Y, et al. Small molecule inhibition of cGAS reduces interferon expression in primary macrophages from autoimmune mice. Nat Commun. 2017;8(1):750.

23. Gaidt MM, Ebert TS, Chauhan D, Ramshorn K, Pinci F, Zuber S, et al. The DNA Inflammasome in Human Myeloid Cells Is Initiated by a STING-Cell Death Program Upstream of NLRP3. Cell. 2017;171(5):1110-24 e18.

24. Basiorka AA, McGraw KL, Abbas-Aghababazadeh F, McLemore AF, Vincelette ND, Ward GA, et al. Assessment of ASC specks as a putative biomarker of pyroptosis in myelodysplastic syndromes: an observational cohort study. Lancet Haematol. 2018;5(9):e393-e402.

25. Skourti-Stathaki K, Proudfoot NJ, Gromak N. Human senataxin resolves RNA/DNA hybrids formed at transcriptional pause sites to promote Xrn2-dependent termination. Mol Cell. 2011;42(6):794-805.

26. Koo CX, Kobiyama K, Shen YJ, LeBert N, Ahmad S, Khatoo M, et al. RNA polymerase III regulates cytosolic RNA:DNA hybrids and intracellular microRNA expression. The Journal of biological chemistry. 2015;290(12):7463-73.

27. Yip BH, Steeples V, Repapi E, Armstrong RN, Llorian M, Roy S, et al. The U2AF1S34F mutation induces lineage-specific splicing alterations in myelodysplastic syndromes. J Clin Invest. 2017;127(6):2206-21.

28. Madan V, Han L, Hattori N, Teoh WW, Mayakonda A, Sun QY, et al. ASXL2 regulates hematopoiesis in mice and its deficiency promotes myeloid expansion. Haematologica. 2018;103(12):1980-90.

29. Smeets MF, Tan SY, Xu JJ, Anande G, Unnikrishnan A, Chalk AM, et al. Srsf2(P95H) initiates myeloid bias and myelodysplastic/myeloproliferative syndrome from hemopoietic stem cells. Blood. 2018;132(6):608-21.

30. Moran-Crusio K, Reavie L, Shih A, Abdel-Wahab O, Ndiaye-Lobry D, Lobry C, et al. Tet2 loss leads to increased hematopoietic stem cell self-renewal and myeloid transformation. Cancer Cell. 2011;20(1):11-24.

31. Zhang P, Behre G, Pan J, Iwama A, Wara-Aswapati N, Radomska HS, et al. Negative cross-talk between hematopoietic regulators: GATA proteins repress PU.1. Proc Natl Acad Sci U S A. 1999;96(15):8705-10.

32. Tyrkalska SD, Perez-Oliva AB, Rodriguez-Ruiz L, Martinez-Morcillo FJ, Alcaraz-Perez F, Martinez-Navarro FJ, et al. Inflammasome Regulates Hematopoiesis through Cleavage of the Master Erythroid Transcription Factor GATA1. Immunity. 2019;51(1):50-63 e5.

33. Jaiswal S, Fontanillas P, Flannick J, Manning A, Grauman PV, Mar BG, et al. Age-related clonal hematopoiesis associated with adverse outcomes. N Engl J Med. 2014;371(26):2488-98.

34. Fuster JJ, MacLauchlan S, Zuriaga MA, Polackal MN, Ostriker AC, Chakraborty R, et al. Clonal hematopoiesis associated with TET2 deficiency accelerates atherosclerosis development in mice. Science (New York, NY). 2017;355(6327):842-7.

35. Zhou R, Xie X, Qin Z, Li X, Liu J, Li H, et al. Cytosolic dsDNA is a novel senescence marker associated with pyroptosis activation. Tissue Cell. 2021;72:101554.

36. De Maria R, Zeuner A, Eramo A, Domenichelli C, Bonci D, Grignani F, et al. Negative regulation of erythropoiesis by caspase-mediated cleavage of GATA-1. Nature. 1999;401(6752):489-93.

37. Hamarsheh S, Osswald L, Saller BS, Unger S, De Feo D, Vinnakota JM, et al. Oncogenic Kras(G12D) causes myeloproliferation via NLRP3 inflammasome activation. Nat Commun. 2020;11(1):1659.

38. Muto T, Walker CS, Choi K, Hueneman K, Smith MA, Gul Z, et al. Adaptive response to inflammation contributes to sustained myelopoiesis and confers a competitive advantage in myelodysplastic syndrome HSCs. Nat Immunol. 2020;21(5):535-45.

39. Yamaguchi N, Oyama M, Kozuka-Hata H, Inoue J. Involvement of A20 in the molecular switch that activates the non-canonical NF-small ka, CyrillicB pathway. Sci Rep. 2013;3:2568.

40. Parvatiyar K, Pindado J, Dev A, Aliyari SR, Zaver SA, Gerami H, et al. A TRAF3-NIK module differentially regulates DNA vs RNA pathways in innate immune signaling. Nat Commun. 2018;9(1):2770.

41. Weinreb JT, Ghazale N, Pradhan K, Gupta V, Potts KS, Tricomi B, et al. Excessive R-loops trigger an inflammatory cascade leading to increased HSPC production. Dev Cell. 2021;56(5):627-40.e5.

42. Kim E, Ilagan JO, Liang Y, Daubner GM, Lee SC, Ramakrishnan A, et al. SRSF2 Mutations Contribute to Myelodysplasia by Mutant-Specific Effects on Exon Recognition. Cancer Cell. 2015;27(5):617-30.

43. Ko M, Bandukwala HS, An J, Lamperti ED, Thompson EC, Hastie R, et al. Ten-Eleven-Translocation 2 (TET2) negatively regulates homeostasis and differentiation of hematopoietic stem cells in mice. Proc Natl Acad Sci U S A. 2011;108(35):14566-71.

44. Wang GG, Calvo KR, Pasillas MP, Sykes DB, Häcker H, Kamps MP. Quantitative production of macrophages or neutrophils ex vivo using conditional Hoxb8. Nature methods. 2006;3(4):287.

45. Heckl D, Kowalczyk MS, Yudovich D, Belizaire R, Puram RV, McConkey ME, et al. Generation of mouse models of myeloid malignancy with combinatorial genetic lesions using CRISPR-Cas9 genome editing. Nature biotechnology. 2014;32(9):941.

46. Lage SL, Dominical VM, Wong CS, Sereti I. Evaluation of Canonical Inflammasome Activation in Human Monocytes by Imaging Flow Cytometry. Front Immunol. 2019;10:1284.

47. Chuang MK, Chiu YC, Chou WC, Hou HA, Chuang EY, Tien HF. A 3-microRNA scoring system for prognostication in de novo acute myeloid leukemia patients. Leukemia. 2015;29(5):1051-9.

Figure Legends:

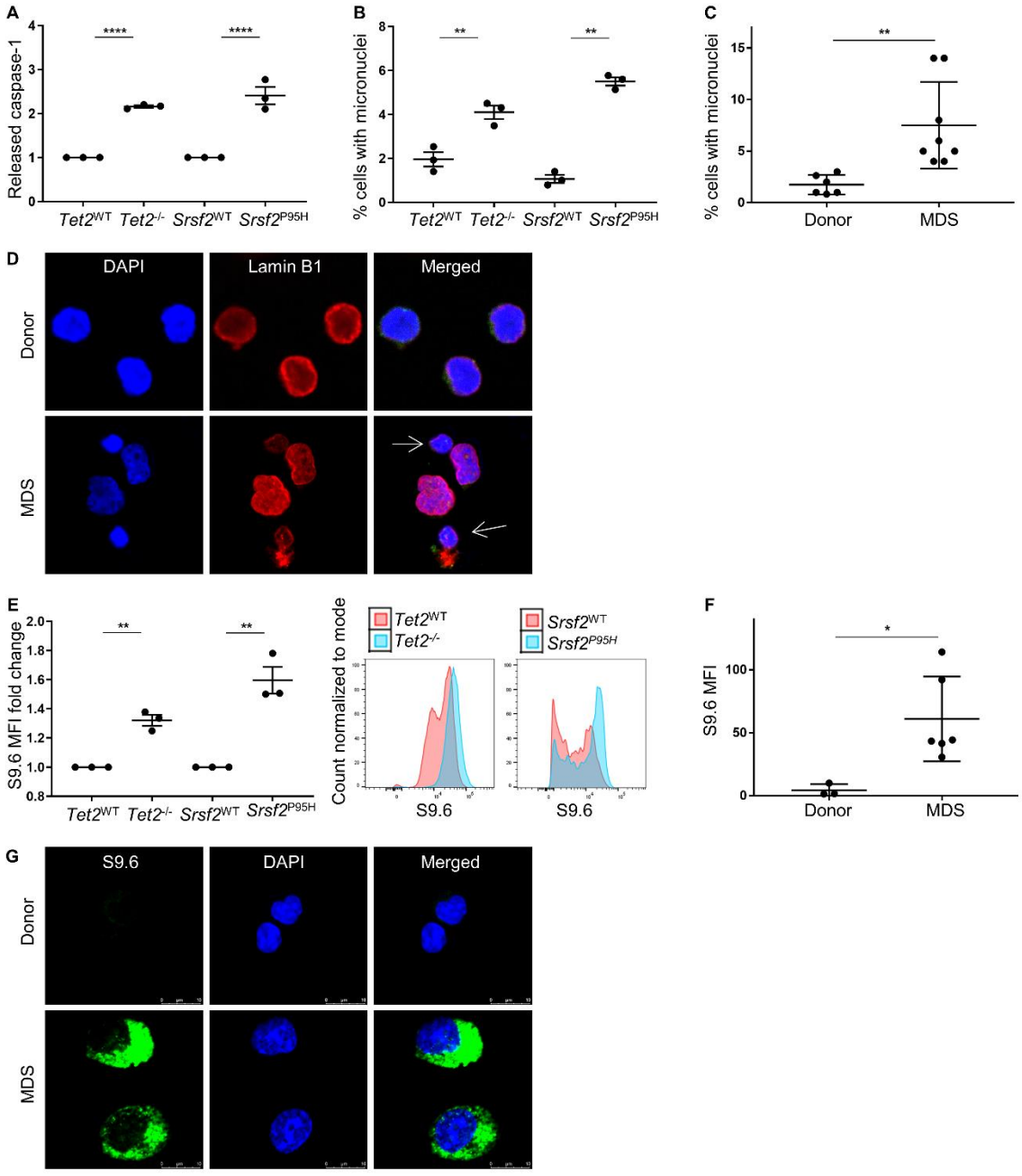

Figure 1. Cytosolic DNA is increased in MDS bone marrow and murine SGM models. (A) Released caspase-1 is significantly increased in SGM mutant cell lines compared to WT controls, assessed by GloMax assay (n = 3 each). (B) Percent of cells with micronuclei is significantly increased in SGM cell lines compared to wildtype controls (n = 3 each), as well as in MDS patient BM-MNCs (n = 8) compared to bone marrow donors (n = 6) (C). (D) Representative immunofluorescence images of micronuclei in MDS (n = 8) compared to donor BM-MNCs (n = 6). (E) R-loops expression measured by S9.6 flow cytometry is significantly increased in SGM cell lines compared to wildtype controls (n = 3 each) as well as in MDS BM-MNCs (n = 6) compared to controls (n = 3) with representative histograms. (F) Quantification of immunofluorescent images (G) of R-loops (green) in MDS (n = 6) compared to donor BM-MNCs (n = 3). Data is presented as mean +/- SEM *: Student t-test, P≤0.05, **: P≤0.01, ***: P≤0.001, ****: P≤0.0001

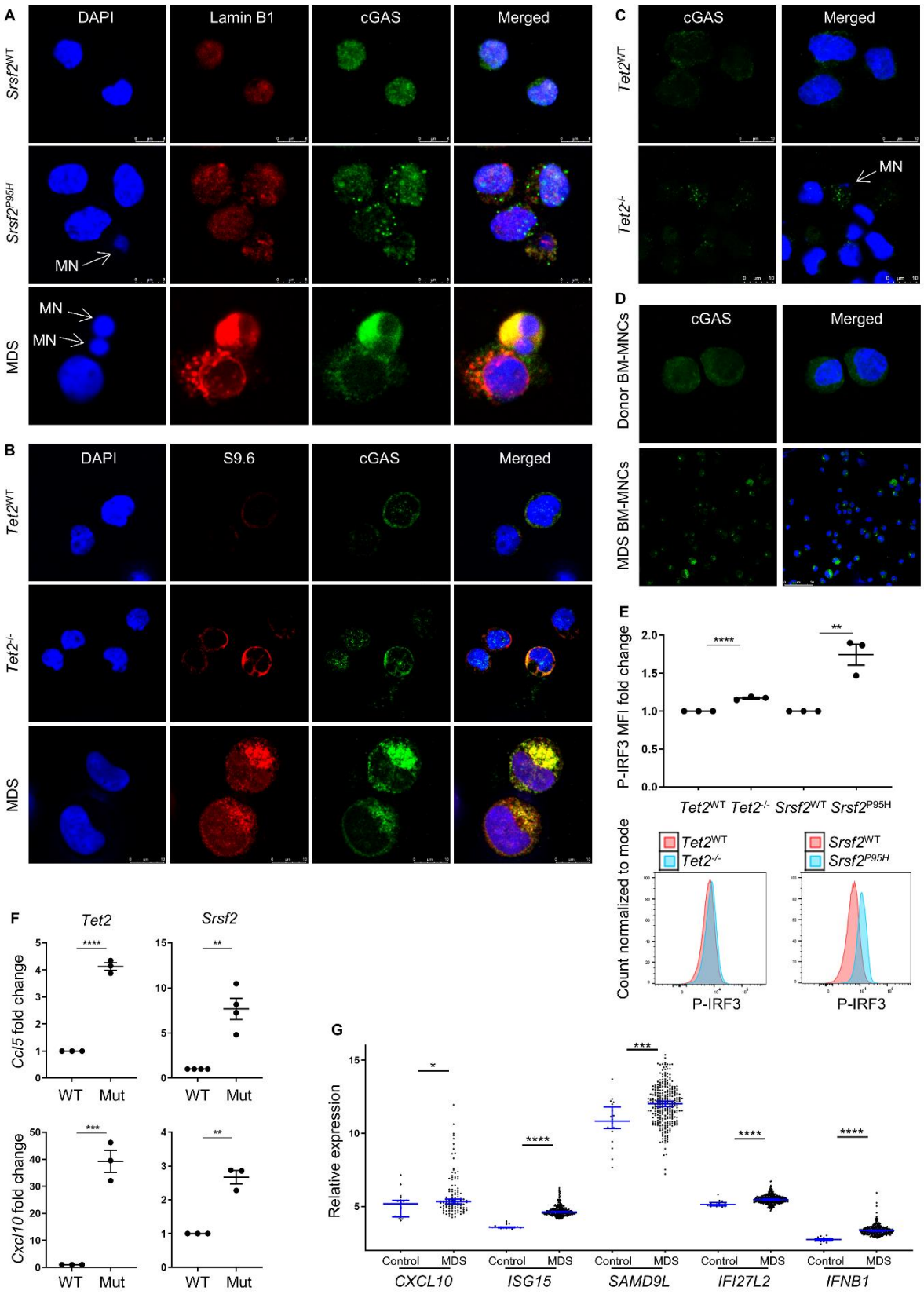
A
DAPI
Lamin B1
cGAS
Merged
Srsf2WT
Srsf2P95H
MN
MDS
MN
MN
B
DAPI
S9.6
cGAS
Merged
Tet2WT
Tet2-/-
MDS
C
cGAS
Merged
Tet2WT
Tet2-/-
MN
D
cGAS
Merged
Donor BM-MNCs
MDS BM-MNCs
E
P-IRF3 MFI fold change
2.0
1.5
1.0
0.5
0.0
****
**
Tet2WT Tet2-/- Srsf2WT Srsf2P95H
Count normalized to mode
Tet2WT
Tet2-/-
Srsf2WT
Srsf2P95H
P-IRF3
P-IRF3
F
Tet2
Srsf2
Ccl5 fold change
Cxcl10 fold change
****
**
***
**
WT
Mut
G
Relative expression
*
***
****
****
****
Control
MDS
CXCL10
ISG15
SAMD9L
IFI27L2
IFNB1

Figure 2. cGAS is activated in somatic gene mutation models and MDS bone marrow cells (A) Representative immunofluorescence images of SGM mutant cell lines and MDS BM-MNCs with colocalization of cGAS to micronuclei with compromised nuclear membranes. (B) Representative immunofluorescence images of colocalization of cGAS and R-loops in SGM mutant cell lines and MDS BM-MNCs. (C) Aggregation of cGAS foci is increased in mutant immortalized SGM cells compared to wildtype controls (cGAS green, DAPI blue; 3780x,). (D) Aggregation of cGAS in MDS BMMCs (630x) compared to donor BMMCs (2940x) (E) Phospo-IRF3 is increased in SGM models compared to WT controls, representative flow histograms (n = 3 each). (F) ISG expression is increased in the immortalized SGM cells compared to WT controls (n = 3 each) . (G) ISG and *IFNB1* expression is significantly increased in MDS BM-MNCs (n = 213) compared to age matched donors (n = 20). Data are presented as mean +/- SEM. Images are representative of at least 2 independent experiments Student t-test for in vitro data; Mann-Whitney U test for (G), *: P≤0.05, **: P≤0.01, ***: P≤0.001, ****: P≤0.0001

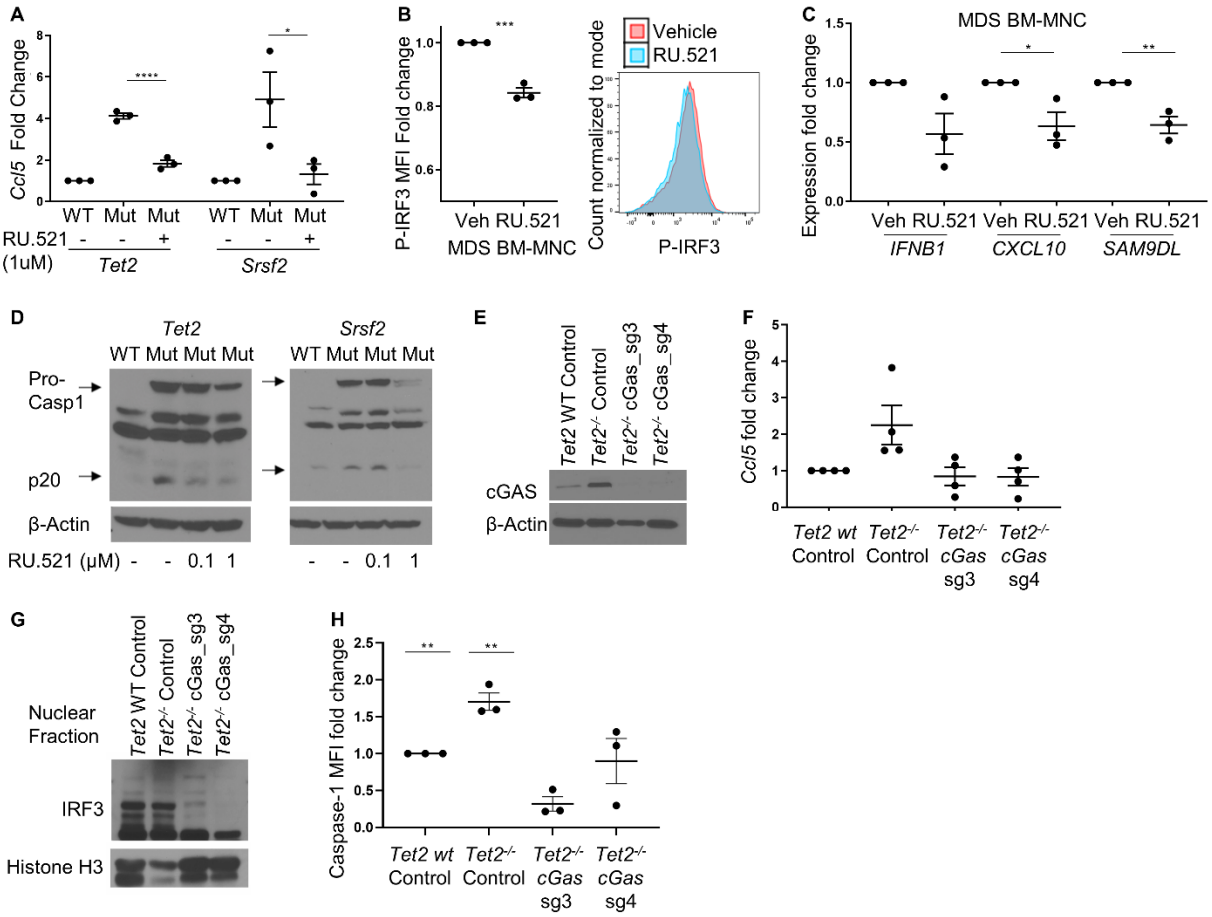
A
Ccl5 Fold Change
WT Mut Mut WT Mut Mut
RU.521 (1uM) - - + - - +
Tet2
Srsf2
B
P-IRF3 MFI Fold change
Veh RU.521
MDS BM-MNC
Count normalized to mode
Vehicle
RU.521
P-IRF3
C
MDS BM-MNC
Expression fold change
Veh RU.521 Veh RU.521 Veh RU.521
IFNB1
CXCL10
SAM9DL
D
Tet2
Srsf2
WT Mut Mut Mut
Pro-Casp1
p20
β-Actin
RU.521 (μM) - - 0.1 1 - - 0.1 1
E
Tet2 WT Control
Tet2-/- Control
Tet2-/- cGas_sg3
Tet2-/- cGas_sg4
cGAS
β-Actin
F
Ccl5 fold change
Tet2 wt Control
Tet2-/- Control
Tet2-/- cGas sg3
Tet2-/- cGas sg4
G
Nuclear Fraction
IRF3
Histone H3
H
Caspase-1 MFI fold change
Tet2 wt Control
Tet2-/- Control
Tet2-/- cGas sg3
Tet2-/- cGas sg4

Figure 3. cGAS activation licenses NLRP3 inflammasome activation.. (A) 24-hour treatment of 1μM RU.521 decreased *Ccl5* expression nearly to wildtype levels in both SGM cell lines (n = 3 each). (B) P-IRF3 assessed by flow with representative histograms and ISG expression (n = 3) (C) INFB1, CXCL10 and SAM9DL expression decreased in low-risk MDS BM-MNCs treated in vitro with 1μM RU.521 for 48 hours (n = 3) (D) Cleaved caspase 1 decreased in SGM models with RU.521 treatment (E) cGAS western blotting of cells treated with scrambled sgRNA (WT and *Tet2*$^{-/-}$ immortalized cells), or cGAS sg_3 or sg_4 (*Tet2*$^{-/-}$) (F) CRISPR knockout of cGAS in the *Tet2* SGM cell line decreased *Ccl5* expression (n = 4) and nuclear IRF3 (G) compared to scrambled control. (H) Active capase-1 assessed by flow cytometry is decreased with cGAS knockdown by CRIPSR (n = 3). Data are represented as mean +/- SEM. Western blots are representative of at least 2 independent experiments. Student t-test; *.P≤0.05, **: P≤0.01, ***: P≤0.001, ****: P≤0.0001

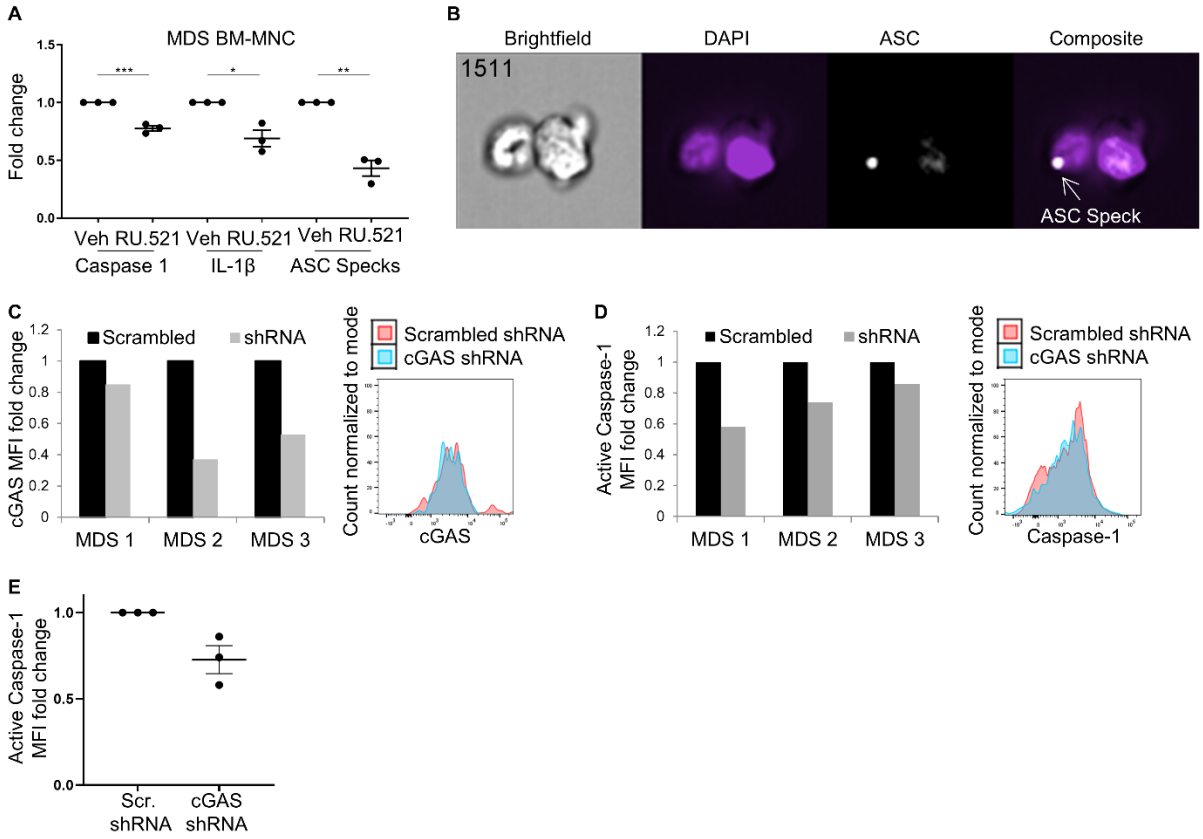
A
MDS BM-MNC
Fold change
1.5
1.0
0.5
0.0
***
*
**
Veh RU.521 Veh RU.521 Veh RU.521
Caspase 1 IL-1β ASC Specks
B
Brightfield
DAPI
ASC
Composite
1511
ASC Speck
C
cGAS MFI fold change
Scrambled
shRNA
MDS 1
MDS 2
MDS 3
Count normalized to mode
Scrambled shRNA
cGAS shRNA
cGAS
D
Active Caspase-1 MFI fold change
Scrambled
shRNA
MDS 1
MDS 2
MDS 3
Count normalized to mode
Scrambled shRNA
cGAS shRNA
Caspase-1
E
Active Caspase-1 MFI fold change
1.0
0.5
0.0
Scr. shRNA
cGAS shRNA

Figure 4. cGAS attenuation inhibits inflammasome activity in primary MDS cells (A) Low-risk MDS BM-MNCs treated in vitro with 1μM RU.521 for 48 hours (n = 3) had decreased active caspase-1, IL-1β, and intracellular ASC specks measured by imaging flow cytometry. (B) Representative image of cell with ASC Speck. (C) Decreased cGAS expression in GFP+ primary bone marrow cells with representative flow histogram (D) Decreased caspase-1 activity in 3 MDS BM-MNC treated with cGAS shRNA with representative flow histogram (E) Average reduction in caspase-1 level of 3 pooled primary MDS specimens treated with shRNA. Data are represented as mean +/- SEM. Student t-test; *: P≤0.05, **: P≤0.01, ***: P≤0.001, ****: P≤0.0001

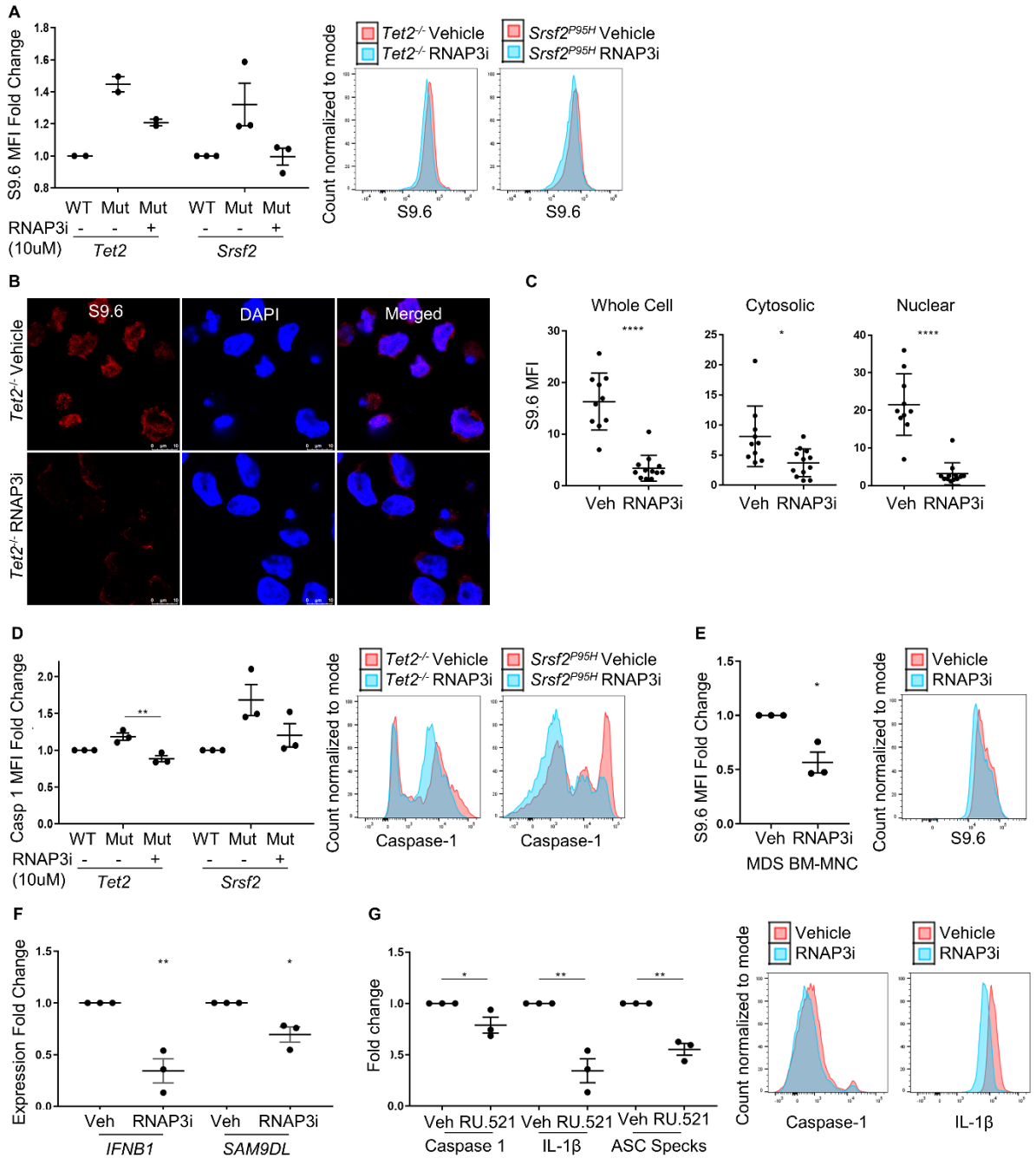
A
S9.6 MFI Fold Change
WT Mut Mut WT Mut Mut
RNAP3i - - + - - +
(10uM) Tet2 Srsf2
Count normalized to mode
Tet2-/- Vehicle
Tet2-/- RNAP3i
Srsf2P95H Vehicle
Srsf2P95H RNAP3i
S9.6
B
S9.6
DAPI
Merged
Tet2-/- Vehicle
Tet2-/- RNAP3i
C
Whole Cell
Cytosolic
Nuclear
S9.6 MFI
Veh RNAP3i
D
Casp 1 MFI Fold Change
Caspase-1
E
S9.6 MFI Fold Change
MDS BM-MNC
Vehicle
RNAP3i
F
Expression Fold Change
IFNB1
SAM9DL
G
Fold change
Veh RU.521
Caspase 1
IL-1β
ASC Specks

Figure 5. RNA Pol 3 inhibition suppresses R-loop accumulation and inflammasome activity. (A) SGM models were treated with ML-60218 (RNAP3i) for 72 hours and R-loop (S9.6) expression was assessed by flow cytometry (n=2 each for *Tet2* cells and n=3 each for *Srsf2* cells) with representative flow histograms (A), (B) Representative IF images of R-loop reduction in *Tet2*$^{-/-}$ immortalized cells treated with RNAP3i, and (C) MFI quantitation of immunofluorescence (n=10 vehicle treated cells and n=12 RNAP3i treated cells). (D) Caspase-1 activity by flow cytometry with representative histograms (n=3 each) (E) Low-risk MDS BM-MNCs treated in vitro with 10μM RNAP3i for 72 hours (n = 3) resulting in a decrease in r-loops with representative histogram, ISGs (n=3 each) (F), and inflammasome markers (Caspase 1, IL1beta, and ASC Specks (n=3 each) (G) with representative flow histograms. Data is presented as mean +/- SEM. Student t-test; *: P≤0.05, **: P≤0.01, ***: P≤0.001, ****: P≤0.0001

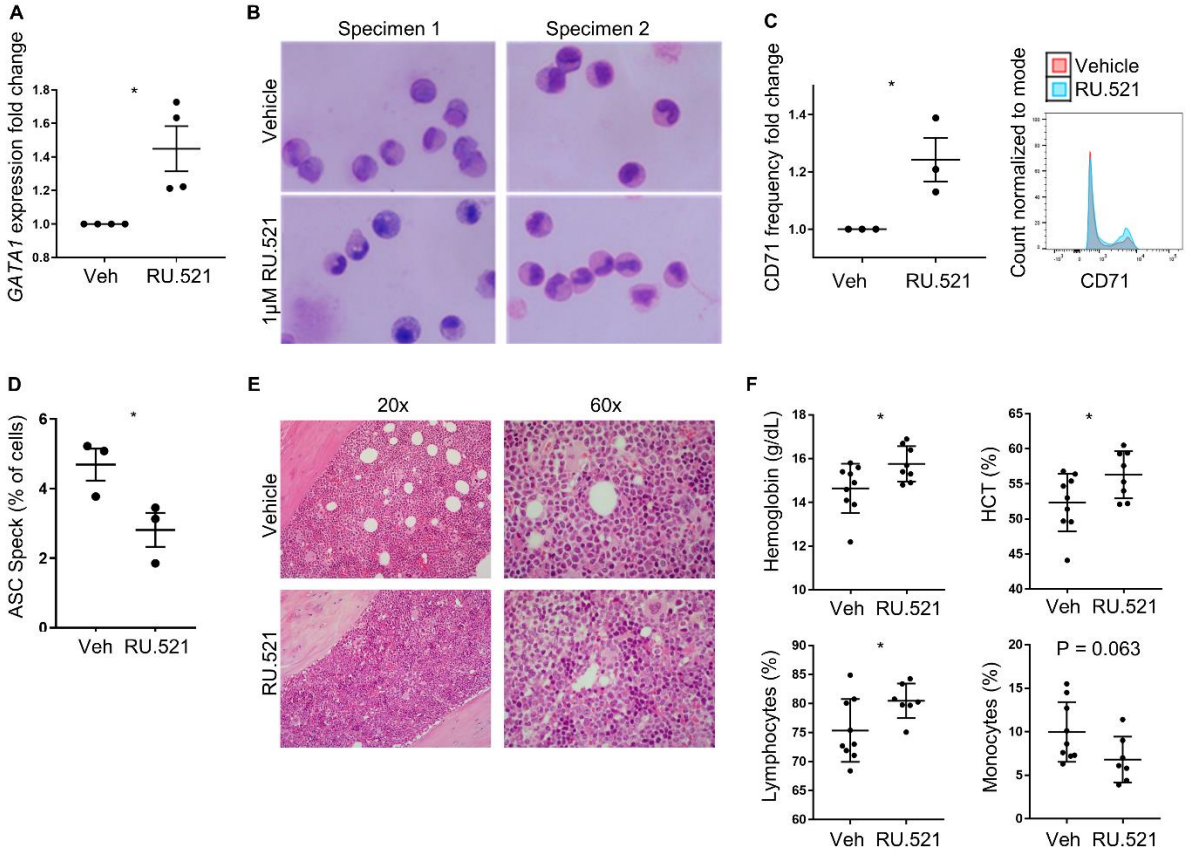
A
GATA1 expression fold change
Veh
RU.521
B
Specimen 1
Specimen 2
Vehicle
1μM RU.521
C
CD71 frequency fold change
Veh
RU.521
Vehicle
RU.521
Count normalized to mode
CD71
D
ASC Speck (% of cells)
Veh
RU.521
E
20x
60x
Vehicle
RU.521
F
Hemoglobin (g/dL)
HCT (%)
Lymphocytes (%)
Monocytes (%)
P = 0.063
Veh
RU.521

Figure 6. Treatment with cGAS inhibitor restores erythroid differentiation. (A) Treatment with the cGAS inhibitor increases *GATA1* transcription (n = 4) in MDS-BMNC, differentiation evidenced by Wright-Geimsa staining (n = 2) (B), and CD71 expression (n = 3), representative flow histogram (C) in MDS BM-MNCs. (D) BM-MNC ASC specks decreased in *Tet2*$^{-/-}$ CD45.2 BMNC treated in vivo for six weeks with RU.521 compared to vehicle (n = 3, each) (E) increased erythroid islands in the bone marrows from mice treated with RU.521compared to mice treated with vehicle, as well as (F) increased hemoglobin, hematocrit, and lymphocytes, and decreased monocytes in treated mice (n = 8) compared to vehicle (n = 9). Data are presented as mean +/- SEM. Student t-test; *: P≤0.05, **: P≤0.01, ***: P≤0.001, ****: P≤0.0001

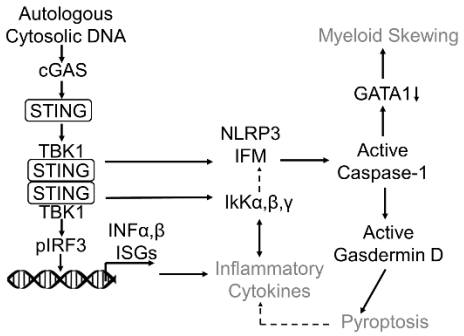
Autologous
Cytosolic DNA
cGAS
STING
TBK1
STING
STING
TBK1
pIRF3
INFα,β
ISGs
NLRP3
IFM
IkKα,β,γ
Inflammatory
Cytokines
Myeloid Skewing
GATA1↓
Active
Caspase-1
Active
Gasdermin D
Pyroptosis

Figure 7. Autologous cytoplasmic DNA activates the cytoplasmic sensor, cGAS, directing inflammasome activation and differentiation defects in MDS. Schematic summarizing cGAS activation as a result of somatic gene mutations that cause accumulation of autologous cytoplasmic DNA and activates cGAS with subsequent inflammasome activity leading to proinflammatory cytokine elaboration, pyroptotic cell death, and hematopoietic stem and progenitor cell differentiation defects.